3D printable lignin-caprolactone material

Kassaun, Banchamlak Bemerw; Wang, Luyao; Backman, Oskar; Xu, Chunlin; Fatehi, Pedram

Published in:
Green Chemistry

DOI:
10.1039/D4GC06179A

Published: 07/04/2025

Document Version
Final published version

Document License
CC BY-NC

Volume 27
Number 13
7 April 2025
Pages 3367-3592

Green Chemistry

Cutting-edge research for a greener sustainable future

rsc.li/greenchem

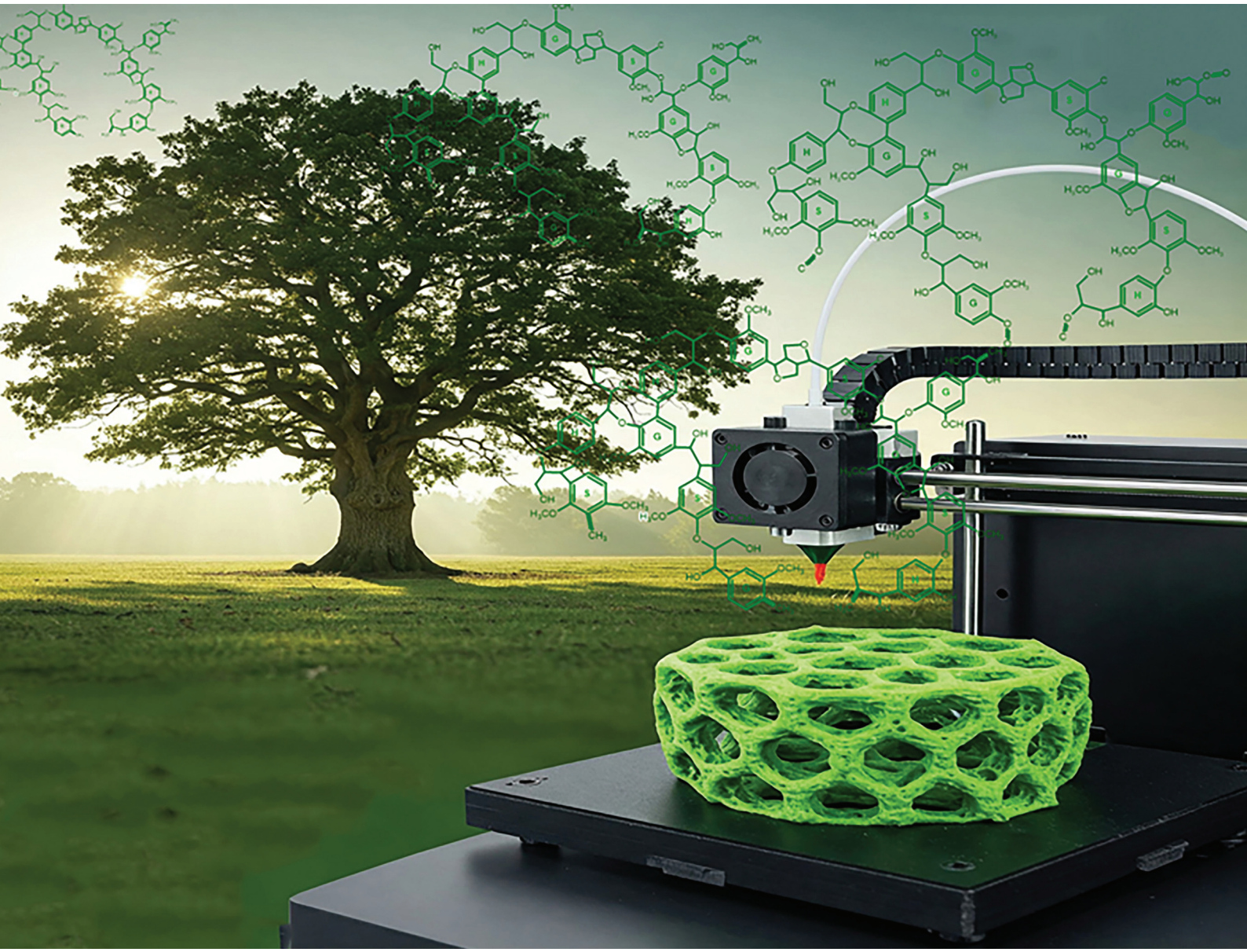

ISSN 1463-9262

ROYAL SOCIETY OF CHEMISTRY

PAPER
Chunlin Xu, Pedram Fatehi *et al.*
3D printable lignin-caprolactone material

25 YEARS ANNIVERSARY

Green Chemistry

PAPER

View Article Online
View Journal | View Issue

Cite this: *Green Chem.*, 2025, **27**, 3451

3D printable lignin-caprolactone material†

Banchamlak Bemerw Kassaun,[a,b] Luyao Wang,[b] Oskar Backman,[b] Chunlin Xu *[b] and Pedram Fatehi *[a,b]

The use of lignin in three-dimensional (3D) printing materials has been considered a viable strategy to generate sustainable 3D printing objects. However, complex molecular structures, high viscosity, and charring of lignin impair its 3D printability. This study investigated the synthesis of lignin-caprolactone polymer and its fused deposition modeling (FDM)-3D printing performance. Lignin-caprolactone polymerization was carried out with ethanol-soluble fractionated birch alkali lignin (L_E) and caprolactone (CL). Results showed that ethanol fractionation reduced lignin's molecular weight from 22 870 to 3827 g mol^{-1} and increased its hydroxyl group concentration. The melt temperature, viscosity, and polymerization degree were considered in the Box-Behnken surface approach to obtain lignin-caprolactone with the best results. Compared to unfractionated lignin caprolactone (LPO), fractionated lignin-caprolactone polymer (L_EPO) had a 10.9% higher grafting ratio, 69.43% rise in melt temperature (T_m), and 85.71% increase in glass transition temperature. The melt rheological investigation showed that L_EPO's lower viscosity (160.9 Pa s) and shear-thinning behavior than those of LPO made it more suitable for the 3D printing application. The 15 °C delay in G' and G'' crossover points of L_EPO compared to LPO improved 3D printing adhesion layers. Furthermore, L_EPO exhibited superior mechanical characteristics and a greater water contact angle (92°) than LPO. The reduction in molecular weight distribution of lignin (due to ethanol fractionation) prior to copolymerization facilitated the production of a 3D-printable polymer containing 75% lignin. By tailoring the melt and viscosity parameters of the lignin-caprolactone copolymer, the lignin-copolymer exhibited improved 3D printing performance, which offers advantages over lignin composite 3D printing.

Received 5th December 2024,
Accepted 18th February 2025

DOI: 10.1039/d4gc06179a

rsc.li/greenchem

Green foundation

1. This work introduces a simple molecular weight upgrading and a solvent-free polymerization reaction (*i.e.*, a green process) to fabricate a sustainable polymer (lignin-caprolactone, LCP, polymer) with outstanding characteristics that are suitable for 3D printing.
2. This work illustrates that, by fractionating lignin and controlling its molecular weight, it is possible to generate LCP that contains a large proportion of lignin derivative (>75 wt%) and has excellent thermal and rheological properties, which can be readily used for 3D printing excluding the necessity of other chemicals in the 3 D printing formulation.
3. In future work, other lignin fractionation processes may be explored to mimic the molecular weight of lignin so that a larger proportion of lignin can be used in 3D printing material fabrication.

1. Introduction

Fused deposition modeling (FDM) is a widely used extrusion-based technique for fabricating 3D printing materials.[1,2] Generally, rheological properties, thermal conductivity, and shear rate influence polymeric materials' printability *via* FDM.[3] Currently, acrylonitrile butadiene styrene, polyethylene terephthalate, polycarbonate, polyether ether ketone, polypropylene, polylactic acid, and nylon are commonly used in FDM-3D printing.[4,5] Despite their high efficiency, they are environmentally unfriendly and expensive.[2] Thus, the incentive for generating sustainable 3D printing material is high.

The use of various biomass materials in 3D printing, such as cellulose and hemicellulose, has gained attention due to their renewable nature and potential to reduce environmental impacts.[6,7] These materials have been utilized to produce bio-

[a]*Department of Chemical Engineering, Lakehead University, 955 Oliver Road, Thunder Bay, ON P7B 5E1, Canada. E-mail: pfatehi@lakeheadu.ca*
[b]*Laboratory of Natural Materials Technology, Faculty of Science and Engineering, Åbo Akademi University, Henrikinkatu 2, Turku, FI-20500, Finland. E-mail: chunlin.xu@abo.fi*

† Electronic supplementary information (ESI) available. See DOI: https://doi.org/10.1039/d4gc06179a

degradable composites for fabricating 3D printed components, which provide advantages for sustainable manufacturing.[8] Nevertheless, the usability of cellulose and hemicellulose in 3D printing in the FDM technique is limited owing to their low-temperature stability, moisture sensitivity, weak mechanical properties, and challenges in extrusion caused by their fibrous nature.[9] Thanks to its high thermal stability, moisture resistance, higher mechanical properties, antioxidant, antibacterial, and biodegradable properties, lignin, *i.e.*, a plentiful and sustainable biopolymer, has gained attention for fabricating sustainable 3D printing materials.[10,11]

Lignin has traditionally been underutilized and dominantly burnt as an energy source.[12] Its rich aromatic structure makes it suitable for creating valuable products, such as bioadhesives, bioplastics, and carbon fibers.[13,14] Nevertheless, the complex structure of lignin, its undesired thermal properties (*e.g.*, its ability to char at high temperatures), and rheological properties (*e.g.*, shear thickening behavior, which causes increased resistance to flow or deformation) have hindered its application in 3D printing applications.[15–17] For this reason, the application of lignin in 3D printing *via* FDM is limited to lignin being blended at a low quantity (*e.g.*, 2–40%) with other polymers, such as acrylonitrile-butadiene-styrene (ABS), polylactic acid (PLA) and polyamide (PA).[17–20]

The source and extraction process of lignin also influences its applicability in FDM 3D printing. Alkali hardwood lignin is especially beneficial compared to the softwood kraft lignin because of its less structural variability, which mitigates the risk of nozzle blockage.[21,22] For example, Nguyen *et al.* mixed hardwood lignin and thermoplastic nylon 12 and reported improved rigidity and decreased melting viscosity of lignin for use as a 3D printing material.[17] In another study, an organosolv hardwood lignin exhibited high compatibility with polylactic acid (PLA), and its 15 wt% lignin-loaded composition exhibited outstanding printability *via* the FDM process.[15] While incorporating lignin into polymer blends offers advantages, the exceptional properties (*e.g.*, mechanical stability, UV protection, and antioxidant) of lignin in the blend are constrained by the percentage of lignin (40 wt% max) in the matrix.[23,24] Additionally, the blending process frequently results in phase separation, further restricting the ultimate characteristics of the printed material. One way to widen the use of lignin in a 3D printable formulation is to crosslink lignin and other thermoplastic polymers to improve their thermal and rheological properties. The performance of polymerized lignin in 3D printing applications has yet to be explored. The present work examined polymerizing lignin with caprolactone (CL) to generate sustainable 3D printing material as the first objective.

Polycaprolactone (PCL) is a biodegradable polyester with a low melting point of approximately 60 °C and a glass transition temperature of roughly −60 °C.[25,26] PCL is a favorable thermoplastic polymer for producing FDM scaffolds for tissue engineering applications due to its biocompatibility, biodegradability, low melting temperature, low glass transition temperature, and high thermal stability.[27,28] Generally, carbon nanotubes, pristine graphene, and tricalcium phosphate are included in the PCL matrix to improve the mechanical properties and structural integrity of PCL materials.[29–31] However, these fillers would limit their biodegradability and biocompatibility.[32] In the past, caprolactone (CL), the monomer for PCL, was polymerized with kraft lignin to produce thermoplastic materials by compression molding with PCL.[33] However, the report did not elaborate on the reaction fundamentals and the molding characteristics of the lignin-caprolactone polymer. As the characteristics of such polymers would significantly impact their 3D printing affinity, the second objective of this study was to understand the polymerization reaction system to achieve a sustainable polymer with the best printing performance.

In this study, the lignin was fractionated by ethanol to reduce its molecular weight before polymerizing with CL.[34,35] Ethanol fractionation is chosen for upgrading lignin properties (*e.g.*, molecular weight distribution) due to its simplicity, less severe process conditions, and the specific solubility of lignin in ethanol, as opposed to other techniques, such as lignin depolymerization and acid catalytic upgrading.[36–40] This study presents a ring-opening polymerization of birch alkali lignin (L) and CL to produce a 3D printable polymer with exceptional flow characteristics. The properties of L were improved using ethanol fractionation, and the ethanol soluble fractionated lignin (L_E) resulted in a lower molecular weight than L, which was then used to fabricate lignin-caprolactone polymer with best properties (L_EPO) following the Box-Behnken (BBD) response surface method (RSM). The printability of the selected sample was assessed by running melt rheology. Then, the 3D printing methods of FDM were employed to study the 3D printing performance of the generated sustainable material. The mechanical strength, surface properties, and appearance of 3D-printed structures were evaluated comprehensively. This work demonstrated a promising approach to utilizing polymerized lignin for a microstructurally well-organized 3D printed material fabrication.

2. Method and materials

2.1. Materials

Birch alkali lignin (BL) was supplied by CH-Bioforce Oy (Espoo, Finland), ethanol (96%), hexane (99%), ε-caprolactone (CL), dibutyltin dilaurate (DBTDL, 95%), methanol (95%), dimethyl sulfoxide (DMSO-d_6), chloroform ($CDCl_3$), anhydrous pyridine, *endo-N*-hydroxy-5-norbornene-2,3-dicarboximide, chromium(III) acetylacetonate ($Cr(acac)_3$), 2-chloro-4,4,5,5-tetramethyl-1,3,2-dioxaphospholane (Cl-TMDP), dimethyl sulfoxide-d_6 (DMSO-d_6), chloroform-d containing 0.03%, tetramethylsilane (TMS), and polycaprolactone (PCL, 80 000 g mol^{-1}) were purchased from Sigma Aldrich.

2.2. Ethanol fractionation of birch alkali lignin

Birch alkali lignin (L) was fractionated using ethanol. The amount of solvent and lignin was set to 7 : 1 wt/wt (70 g of

ethanol for 10 g of lignin). After stirring for 2 h, the insoluble and soluble parts of lignin were separated using a vacuum filter. The ethanol-soluble part of lignin (L_E) was taken and treated by a rotary evaporator to separate lignin from ethanol. Subsequently, samples were collected, washed with hexane (20 mL) to remove the extractives, and dried in a 60 °C oven for 48 hours. Eqn (S1) (ESI)† was used to measure the yield of the lignin fractionation process.

2.3. Experimental design by box-Behnken (BBD)- response surface method (RSM) for lignin-caprolactone (L_EP) polymerization

The experiments for the polymerization of lignin and caprolactone (L_EP) were designed using response surface methodology (RSM) based on a box-Behnken design (BBD). The BBD-RSM approach was used to evaluate the impact of three independent factors on the L_EP polymer's viscosity and melt temperature. To accomplish this goal, the influence of three experimental factors (the ratio of caprolactone monomer to the hydroxyl group of lignin (CL/OH), the concentration of catalyst, and the reaction duration) was assessed. These factors were evaluated at three levels: low, medium, and high, represented by coded values of −1, 0, and +1, respectively, in Table S1.† To achieve this objective, 17 experiments were devised using the Box-Behnken Design (BBD) methodology. All second-order regression coefficients were determined by the statistical analysis of the findings using the ANOVA technique. Afterward, the best reaction conditions were determined by merging the acquired outcomes and graphing an equation for each response variable. The statistical analysis of multivariable equations, derivation of coefficients for a second-order regression model, and the examination of the impacts of factors on variables were conducted using design expert statistical software (Version 12, State-Ease Inc, USA). All BBD-RSM equations are listed in eqn (S2)–(S5).†

2.4. Polymerization of lignin and caprolactone

Lignin and caprolactone polymerization generates lignin caprolactone polymer (L_EP) without the need for a solvent.[33] Caprolactone was used as a monomer for ring-opening polymerization (ROP), lignin was used as a micro initiator, and DBTDL was used as a catalyst. The L_E was mixed with CL based on the CL/OH ratio of lignin (as listed in Table S1†) at 50 °C under nitrogen and stirred for 30 min. DBTDL (based on the wt% ratio of lignin listed in Table S1†) was added slowly to the mixture, which was heated to 150 °C under magnetic stirring (250 rpm). ROP is a form of chain-growth polymerization in which the terminal end of a polymer chain acts as a reactive center where further cyclic monomers (CL) can react by opening its ring structure and forming a longer polymer chain. The –COO– group is formed *via* the opening of the CL ring and reacts with the OH group of lignin to form an ester linkage, leaving –OH at the end of the CL chain, which subsequently reacts with CL monomers to grow a PCL (Fig. S1b†). When the reaction was complete (for the durations listed in Table S1†), the product was cooled to room temperature, and the mixture was washed several times with cool methanol to remove impurities. The overall schematics of the reaction are described in Fig. S1a.† The reaction conditions for the samples detailed in the main documents, L_EP2, L_EP5, and L_EP6, are as follows: CL/OH ratios of 2.6, 1.73, and 0.83 mmol g^{-1}, respectively; a reaction time of 420 minutes for all; and catalyst concentrations of 0.5, 0.75, and 1 wt% based on lignin content, respectively (Table S2†). The optimized conditions were a CL/OH ratio (mmol g^{-1}) of 1.1, a reaction time of 420 min, and a catalyst concentration of 1 wt% based on lignin amount (Table S2†), which generated the sample labeled as L_EP. A control sample with unfractionated lignin (L) was produced under the same conditions as L_EPO and labeled as LPO.

2.5. Lignin filament extrusion

Samples prepared under the optimization conditions were used to generate filaments. The lignin caprolactone polymer filament was generated using ethanol-fractionated lignin copolymer under optimized conditions (L_EP), and the control sample was generated by unfractionated lignin under the same conditions and labeled as LP. The L_EP and LP were extruded using a compounding twin extrusion machine (Xplore MC15HT). The extrusion was conducted at 100 °C for LPO and 80 °C for LEPO at a speed of 5 rpm to generate filaments with a 1.5–1.7 mm diameter.

2.6. 3D printing of LPO and L_EPO polymers

The printability of LPO and L_EPO was assessed by the fused deposition modeling (FDM) method using extrusion-based 3D printing (Printer One, BRINTER Ltd, Finland) equipped with a 0.55 mm nozzle diameter. The samples were prepared as a pallet by chopping the prepared filaments and fed to a granular tool printhead with the temperature set at 100 °C for LPO and 80 °C for L_EPO. The print bed was prepared by coating a tin PCL layer for better grip throughout the study. An eight-layered honeycomb structure was printed at a speed of 8 mm s^{-1}, pressure of 200 mbar, layer height of 0.2 mm, and shell thickness of 0.5 mm.

2.7. Characterization of lignin and lignin-caprolactone polymers

2.7.1. Molecular weight analysis. The molecular weight of lignin derivatives (L, L_E) and the copolymers (L_EP2, L_EP5, L_EP6, L_EPO, and LPO) was assessed with a size exclusion chromatography (SEC) equipped with a multiangle light scattering detector and differential refractive index concentration detector (MALLS(IR)). Vacuum oven-dried (40 °C) samples were prepared in a clean HPLC vial at 10 mg mL^{-1} concentration in DMSO/0.05 M LiBr eluent, followed by filtration using 0.2 μm Nylon filters before SEC analysis. The separation was performed on a Jordi Gel glucose mixed-bed guard column (50 mm × 10 mm i.d) and a Jordi Gel GBR mixed-bed column (250 mm × 10 mm i.d). The molecular weight analysis was performed using the following parameters: 0.5 mL min^{-1} flow rate, 60 °C column temperature, 100 μL injection volume, and

0.15 mL g^{-1} dn/dc value. The data was evaluated by Astra software, version 7.3.3.[41]

2.7.2. NMR analysis. The hydroxyl groups of L, L_E, L_EP2, L_EP5, and L_EP6 (reaction conditions available in Table S4†), L_EPO, and LPO were quantified by ^{31}P NMR.[42] The samples were prepared by dissolving 20 mg vacuum oven-dried (40 °C) samples in the solvent mixture of 0.55 mL of anhydrous pyridine and $CDCl_3$ (1.6 : 1, v/v) that contained relaxation reagent of chromium(III) acetylacetone ($Cr(acsac)_3$, 1.3 μmol) and internal standard of *endo-N*-hydroxy-5-norbornene-2-3-dicarboximide (12 μmol). The ratio of internal standard to lignin was set to 0.6 mmol g^{-1}. The hydroxyl groups were phosphorylated with 0.1 mL of 2-chloro-4,4,5,5-tetramethyl-1,3,2-dioxaphospholane for 30 min before ^{31}P-NMR measurement. The concentration of $Cr(acac)_3$ was 0.002 M to ensure the complete relation of the phosphorus nuclei before applying the radiofrequency pulse. Spectrum acquisition parameters were a 10 s pulse delay, 2.0 s acquisition time, and 64 scans. The hydroxyl group was used to calculate the grafting percentage of CL on the hydroxyl group of lignin according to eqn (S6).† ^1H-NMR and HSQC NMR analyses were performed on L, L_E, L_EP, LPO, and L_EPO samples. The ^1H-NMR setup was set to 16 scans, 3.28 s acquisition, 1 s relaxation, and 90° pulse at room temperature. L and L_E samples were prepared by dissolving the vacuum oven-dried (40 °C) samples in 80 mg mL^{-1} DMSO, while L_EP and LPO were prepared by dissolving 80 mg samples in 0.75 mL of $CDCl_3$ (0.03 v/v% of TMS). The HSQC NMR spectra were acquired using the HSQCEDETGPSISP2.3 pulse sequence with a relaxation delay of 2.0 s and an acquisition time of 0.15 s, recording 256 increments of 80 scans per increment. The results were assessed using Top Spin 4.02 software. The ^1H-NMR spectra of the L_EPO and LPO were used to quantify the degree of polymerization (n) in the PCL chain segments, following eqn (S7).† The major linkages of L and L_E were quantified according to eqn (S8) and (S9).†

2.7.3. Thermal analysis. The thermal stability of L, L_E, L_EP (17 samples), L_EPO, and LPO samples was assessed by a Q500 thermogravimetric analyzer (TA Instrument, USA). Around 10 mg of vacuum oven-dried (40 °C) samples were weighed into an alumina disposable crucible (T 2101127, China) and heated from 30 °C to 800 °C at a 10 °C min^{-1} under a nitrogen atmosphere at the flow rate of 15 mL min^{-1}. The samples' glass transition temperature (T_g) and melt temperature (T_m) were assessed using a Discovery DSC 250 calorimeter in a heating–cooling-heating cycle under continuous nitrogen at the flow rate of 15 mL min^{-1}. The vacuum oven-dried (40 °C) samples were weighed into a Tzero pan (T 140829, Switzerland) sealed with a Tzero lid (T 140826, Switzerland) and then transferred to the calorimeter containing a reference, *i.e.*, an empty sealed Tzero pan. TRIOS v5.5.5.1.5 software was used to determine the T_g and T_m of the samples.

2.7.4. Rheology. The viscosity of L_EP (17 samples) was assessed by the BBD-RSM design at each melting temperature using an MCR 702 MultiDrive rheometer (Anton Paar GmbH), a PP25 parallel plate (diameter: 25 mm and gap: 0.5 mm) at a shear rate of 0.1 to 100 s^{-1}. Melt rheological properties of the LPO and L_EPO samples were assessed by temperature ramp experiment at a 1 °C min^{-1} heating rate starting from 130 °C and going to a temperature where the first sight of crossover between storage modulus and loss modulus was detected. The data acquisition time was 10 seconds per data point. In addition, the rheological study was conducted on LPO at a temperature of 100 °C and L_EPO at 80 °C with a hybrid rotational rheometer (Discovery HR-2, TA Instruments, DE, USA). The analysis included a flow ramp test at a shear rate ranging from 0.01 to 1000 s^{-1} and a frequency sweep test of 1 to 100 rad s^{-1}, with a strain of 63% in the viscoelastic zone.

2.7.5. Mechanical properties. The L_EPO films were prepared by molding, and the mechanical properties of the films were examined using universal testing equipment with a 200 N load cell (Shimadzu Instrone-6800 series, Japan). Samples were cut from cast sheets with a rectangular shape die, measuring 27 cm long, 3.12 cm wide (ASTM D638 type V), and 1.2 mm thick. Five specimens from L_EPO film were evaluated at 50 mm min^{-1} and room temperature, and an average value with a standard error was reported. The LPO sample cured faster before the film was properly prepared, and the prepared sample was too brittle to be tested.

2.7.6. Contact angle analysis and imaging. An optical tensiometer assessed the surface wettability of LPO and L_EPO 3D-printed parts using the sessile drop method (Theta Lite, Bolin Scientific, Finland). The experiment was conducted by placing a liquid droplet (6–10 μL) onto the flat side of the 3D-printed samples. The contact angle of the droplet was visually measured using a camera for 10 seconds. The contact angle was analyzed using one-attention software, the measurement was performed in three places, and the mean value was reported. An optical microscope (specifically, a Nikon ECLIPSE E200) was used to capture microscopic photographs of the printed samples.

3. Results and discussion

3.1. Ethanol fractionation of birch alkali lignin

The chemical structure of lignin substantially impacts the characteristics of the material incorporating it.[43] Therefore, the chemical structure, molecular weight, and thermal properties of birch alkali lignin, unfractionated (L) and ethanol fractionated (L_E), were assessed and reported in Fig. 1. The molar mass distributions of L and L_E are illustrated in Fig. 1a. The molecular weight (Mw) and polydispersity ($Đ_M$) values are displayed in Table 1. The L_E exhibited a significantly lower M_w and $Đ_M$ than L. The reduced M_w and $Đ_M$ result from ethanol fractionation, which solubilized part of lignin fragments.[35,44,45]

The ^1H NMR spectra of L and L_E polymers are presented in Fig. 1b. The spectra revealed that aromatic protons appeared in the region of 6.0–7.5 ppm, methoxy proton at 3.75 ppm, aliphatic proton at 0.85–2.2 ppm, and DSMO solvent at 2.5 ppm.[39] L_E showed stronger aliphatic signals that belonged to ethanol residues. The quantity of aliphatic, guaiacyl, C5-substituted, and carboxylic hydroxyl groups in L and L_E was deter-

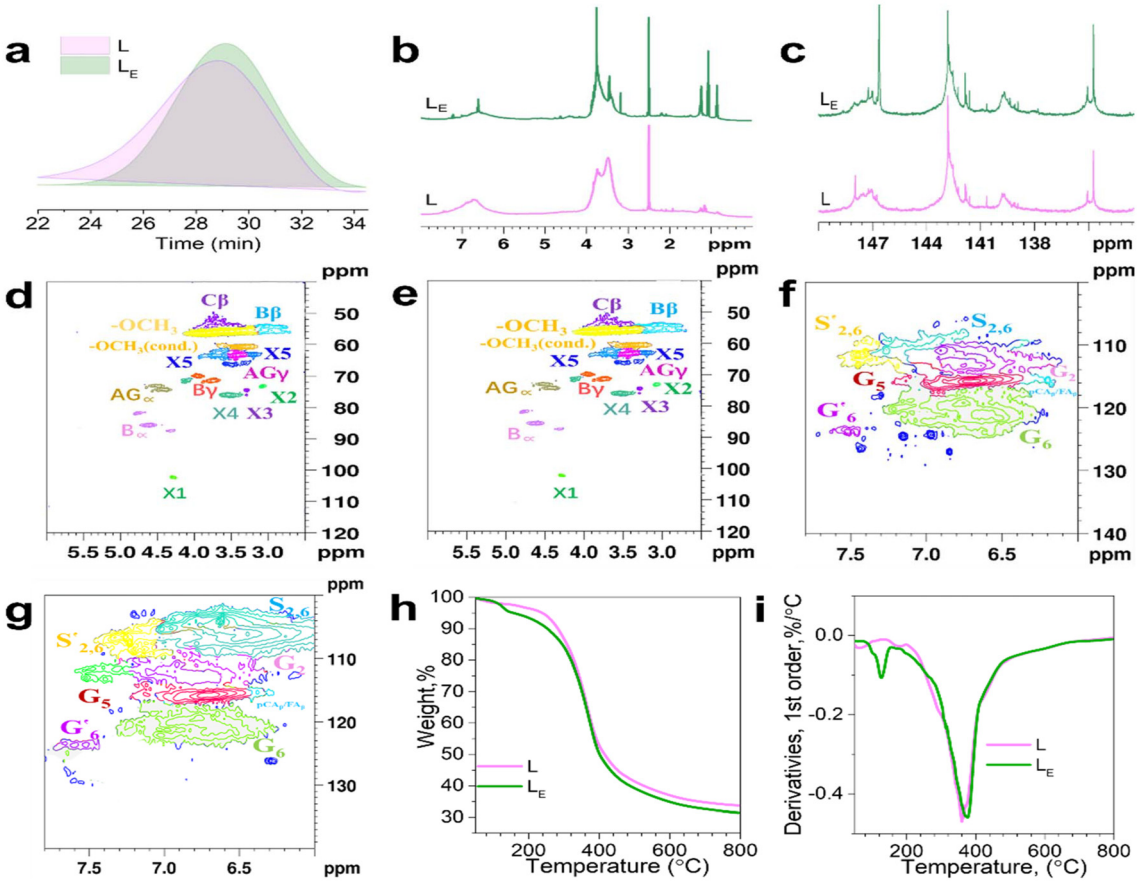

Fig. 1 Molar mass distribution (a), ^{1}H NMR (b), ^{31}P NMR (c), HSQC spectra of oxygenated aliphatic linkages (d and e), aromatic linkages (f and g) of L and LE, and TGA (h) and DTG (i) of L and LE.

mined by quantitative ^{31}P NMR analysis (Fig. 1c), and the hydroxyl group concentration of L and L_E are listed in Table 1. Phenolic hydroxyl groups substantially rose compared to aliphatic and carboxylic hydroxyl groups for LE compared to L. The C_5-substituted hydroxyl groups exhibited the most significant rise from the constituents of phenolic hydroxyl groups. In addition, the interunit linkages and substructures of L and L_E were analyzed by HSQC NMR to understand the changes in lignin structure further. The spectra are presented in Fig. 1(d–g), and the δ_C/δ_H ppm are presented in Table S3.† Quantitative HSQC was used to evaluate the inter-unit linkages in L and L_E using the guaiacol (G2) and syringyl (S2,6) signals as an internal standard described according to eqn (S8) and (S9),† and values are listed in Table 1.[46] The oxygenated aliphatic region (δC/δH 40–120/2.5–6.0) of L and L_E showed signals presented in Fig. 1(d and e). The dominant interunit linkages in L and L_E were the diacylglycerol-β-aryl ether link (β-O-4′) followed by pinoresinol (β–β′) and minor amounts of phenylcoumaran (β-5′). Relative to L, the L_E interunit linkages showed a 165% reduction, which was prominent for β-O-4 (Table 1). This reduction could result from the breakage of β-O-4 linkages due to the ethanol fractionation.[47] This is further supported by the increased phenolic hydroxyl group content from ^{31}P NMR analysis (Fig. 1c). Furthermore, the aromatic linkages (δ_C/δ_H 100–140/6.0–8) were analyzed, and the results are presented in Fig. 1(f and g). The results showed a vigorous intensity of the S units in L_E compared to L. The increase in the S units is consistent with the result of P-NMR, where the phenolic hydroxyl group showed an increase.

The thermal properties of L and L_E were assessed using TGA and DSC to understand the thermal alteration of lignin after ethanol fractionation. The TGA and DTG curves are presented in Fig. 1(h and i). The results indicated that the L_E had a lower T_o (onset temperature) and $T_{50\%}$ (the temperature at which 50% of the weight was lost) than L (Table 1). However, the DTG_{max} of L_E was 20 °C higher than L. The lower molecular weight of L_E than L could be the reason for the lower T_o and $T_{50\%}$. The increased phenolic hydroxyl group of L_E contributed to the higher DTG_{max} due to the higher frequency of intermolecular hydrogen bond interactions of phenolic hydroxyl groups.[48] The glass transition (T_g) of L and L_E were analyzed using DSC, and the results are presented in Table 1. In general, the T_g of L_E was lower than L, which is attributed to the reduced molecular weight, narrower molecular weight distribution (Table 1), and change in the hydroxyl group of L_E, all of which would increase the chain mobility and thus reduce T_g.

Table 1 Yield, grafting ratio (substitution) based on hydroxyl group, molar mass characteristics, hydroxyl group distribution, quantification of major linkages, thermal characteristics, and degree of polymerization (DP) based on H-NMR linkage quantification of lignin and lignin caprolactone polymers

			Molar mass characteristics		Lignin hydroxyl group amount (mmol g^{-1})			The concentration of interunit linkages (% of C9 units)			Thermal characteristics (°C)					
Sample	Yield (wt%)	Grafting (%)	*Mw* (g mol^{-1})	D_M	Total phenolic-OH	Aliphatic-OH	Carboxylic-OH	β-O-4	β–β	β-5	T_o	$T_{50\%}$	DTG_{max}	T_g	T_m	DP
L	100	—	22 870	2.98	2.61	1.38	0.59	229.4	74.1	41.8	239	416	360	120	—	—
L_E	54.2	—	3827	1.00	2.77	1.44	0.64	64.3	27.8	64.3	123	398	380	111.5	—	—
L_EP2	—	48.6	141 600	—	1.25	0.87	0.36	—	—	—	257.8	394.2	400	−20	50	7.02
L_EP5	—	33.6	36 340	—	1.71	1.04	0.47	—	—	—	257.8	404.8	395	−22	52	5.91
L_EP6	—	25.6	38 880	—	2.51	1.00	0.40	—	—	—	266.9	398.4	395	−20	53	4.60
L_EPO	—	26.6	402 300	—	2.13	0.95	0.56	—	—	—	292.2	396.8	396.7	−26	49	4.97
LPO	—	15.7	728 800	—	2.17	0.97	0.69	—	—	—	287.0	391.7	396.6	−14	47	5.16

3.2. Lignin and caprolactone polymerization *via* ring opening polymerization (ROP)

The fractionated lignin (L_E) and caprolactone (CL) polymerization were designed using BBD-RMS. Lignin-(OH) served as a macroinitiator with $Sn(Oct)_2$ catalyst and CL as a monomer.[29] ROP is a polymerization process where the reactive center of a polymer chain is the terminal end. This reactive center allows for the opening of cyclic monomers (CL). It forms a more extended polymer chain (Fig. S1b†).[17,29] The impact of reaction conditions on the response variables (viscosity, melt temperature, and degree of polymerization) is discussed in the ESI with details in Fig. S5, S6 and Tables S5–S7.† This document places particular emphasis on the selected polymers (L_EP2, L_EP5, and L_EP6) and the optimized polymer (L_EPO) and control polymer (LPO).

3.2.1. ^{31}P NMR analysis. According to ^{31}P NMR (Fig. 1b), the total hydroxyl group of L_E was 4.85 mmol g^{-1}. This indicates that about 4.85 mmol g^{-1} of initiating sites are available on the lignin structure, corresponding to 0.64 mmol g^{-1} carboxylic, 1.44 mmol g^{-1} aliphatic, and 2.77 mmol g^{-1} phenolic groups (Table 1). The amount of the hydroxyl group on the lignin-caprolactone polymers after polymerization was assessed by ^{31}P NMR in Fig. 2a. L_EPO, LPO, and 3 selected samples based on the CL/OH ratio (L_EP2, L_EP5, and L_EP6) were analyzed for ^{31}P-NMR spectra in Fig. 2a. The total grafting ratio (substitution) was calculated using the hydroxyl groups of the polymers from ^{31}P-NMR (eqn (S6)†). The results are presented in Table 1. The spectra of lignin-caprolactone polymers showed aromatic and methoxy peaks similar to those of L_E and L. However, the quantification of each peak showed a decrease in all of the hydroxyl groups in the lignin-caprolactone polymers compared to L_E and L in Table 1, confirming the success of polymerization and lignin's hydroxyl group participation in the polymerization. The L_EP2, L_EP5, and L_EP6 samples were chosen from 17 samples to investigate the effect of CL/OH and catalyst concentration on the structure of the polymers. Also, L_EPO (optimized) and LPO (control) were assessed to understand how the structural variations in lignin-caprolactone polymers (due to ethanol fractionation) impact the performance of the copolymer in 3D printing. Interestingly, lignin's hydroxyl groups are present in L_EPO, LPO, L_EP2, L_EP5, and L_EP6, indicating that not all their hydroxyl groups reacted with caprolactone. Table 1 shows the total grafting %, and Fig. S2† shows the substitution percentage for each functional hydroxyl group. L_EPO had a higher grafting and degree of substitution than LPO, as seen in Table 1 and Fig. S2,† respectively.

The increase in the grafting percentage in L_EPO (compared with LPO) is attributed to the increased hydroxyl groups of L_E due to ethanol fractionation (Table 1 and Fig. 1c), creating more initiation sites for the CL ring opening and subsequent grafting. Previous research indicated that the CL monomers would mainly react with the aliphatic hydroxyl groups of kraft lignin, and this reactivity would be dependent on the CL/OH ratios.[49] However, the reactivity of phenolic hydroxyl was

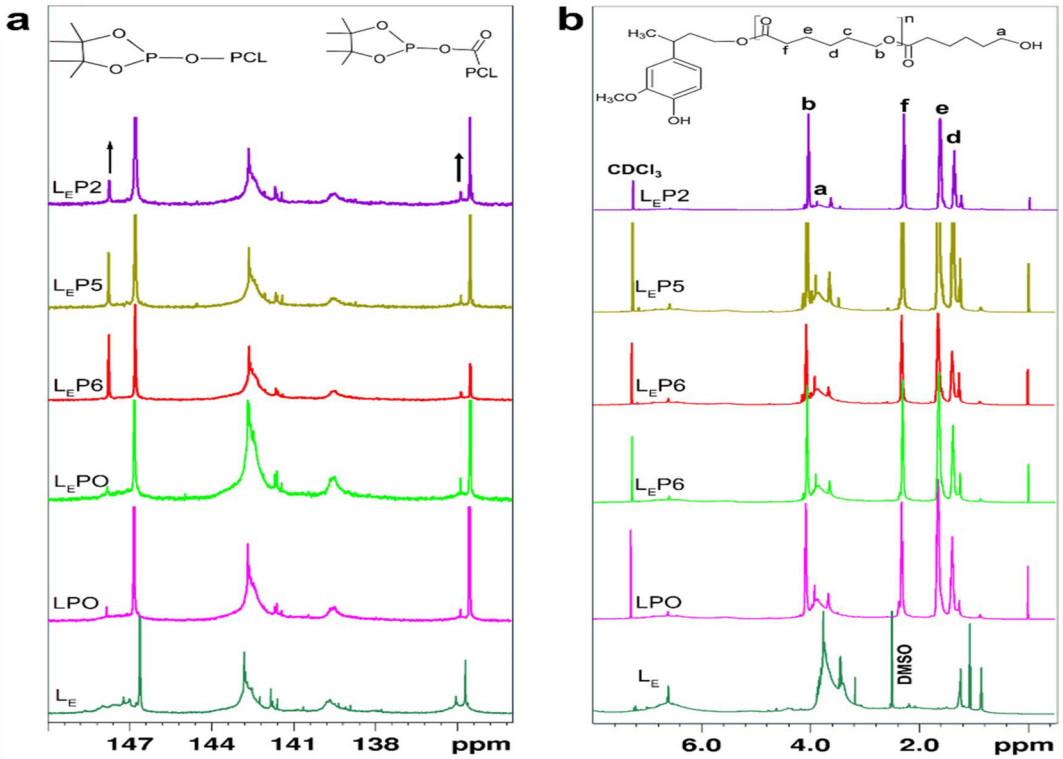

Fig. 2 ^{31}P-NMR (a) and ^{1}H-NMR (b) spectra of LE, LEP's, and LPO polymer.

higher when the ratio of CL/OH was higher.[50] Similarly, L_EP2 had the highest grafting percentage and substitution of phenolic hydroxyl groups (54%), followed by L_EP5 with phenolic hydroxyl groups (38%) between the three samples. This behavior could be due to the higher CL concentration in L_EP2 than in L_EP5, which would provide an advantage in reacting with lignin's hydroxyl sites. L_EP6 had the lowest grafting percentage and the highest substitution of the hydroxyl group (30%).

3.2.2. ^{1}H NMR analysis. The ^{1}H-NMR spectra of the polymers are depicted in Fig. 2b and Fig. S3.† The degree of polymerization (DP) was calculated according to eqn (S7)† and the results are presented in Table S4† and Table 1. The ^{1}H-NMR spectra for all L_EPO, LPO, L_EP2, L_EP5, and L_EP6 samples showed a peak at 7.24 ppm, corresponding to $CDCl_3$, while that at 2.5 ppm corresponded to DMSO in L_E. Due to the chloroform used as the solvent of NMR,[51] the L_EP spectra shifted to the left slightly, moving the methoxy peak from 3.3–3.9 ppm in L_E to 4–4.5 ppm in the lignin-caprolactone polymers. The aliphatic-H of L_E appeared in the 0.5–1.2 ppm range, while that in copolymers was observed at 1.9–2.9 ppm. The aliphatic-H in the copolymers is a result of $-CH_2-$ (d), $-CH_2-$ (e), and $-COCH_2-$ (f) appearing in 1.32, 1.57, and 2.24 ppm, respectively, as they aligned with pure PCL's ^{1}H NMR spectra in Fig. S3.† The signals corresponding to the $-CH_2O-$ (a), –COH (b), the repeating and end-group of the PCL chain at 3.9–4.1 ppm and 3.6–3.7 ppm, respectively, were identified and assigned in the copolymer's spectra. The groups described from ^{1}H-NMR and ^{31}P-NMR spectra (Fig. 2a) and the decrease in the total hydroxyl groups of the lignin (Table 1) confirm the polymerization of CL into PCL on the lignin backbone. Furthermore, the degree of polymerization (DP) calculation following eqn (S7)† revealed that LPO's degree of polymerization (DP) was higher than L_EPO's. This could be related to the fact that the PCL chain in LPO was larger than that in L_EPO, which might be caused by the competing hydroxyl groups in L_E preventing the chain growth. In contrast, the scarcity of hydroxyl groups in L helps the development of the PCL chain. L_EP2 had the highest DP within the three samples, whereas L_EP6 had the lowest (Table S4 and Fig. S3†). This indicates that the CL/OH ratio and catalyst concentration influenced the DP of lignin caprolactone polymers, which was consistent with the grafting percentage for L_EP2 (Table 1).

3.2.3. HSQC NMR analysis. The aromatic and aliphatic regions' C–H correlation signals were assessed by HSQC NMR spectra for L_EP2, L_EP5, L_EP6, L_EPO, and LPO. The results are presented in Fig. 3. The L_EP2, L_EP5, L_EP6, and L_EPO polymers share similar linkages with L_E in the oxygenated aliphatic region $\delta C/\delta H$ 50–100/2.5–5 ppm (Fig. 1d). The aliphatic region ($\delta C/\delta H$ 10–80/0.5–2.5) resulting from the PCL chain appeared dominant in the lignin-caprolactone polymers, which did not appear in L_E (Fig. 1d). The strong aliphatic signals dominating the HSQC NMR spectra (Fig. 3) caused shielding, making the identification of some aliphatic linkage signals hard. The aromatic linkages of $S_{2,6}$, $S'_{2,6}$, G_2, G_5, and G_6 are depicted in Fig. 3b. The LPO's aliphatic oxygenated region and aliphatic

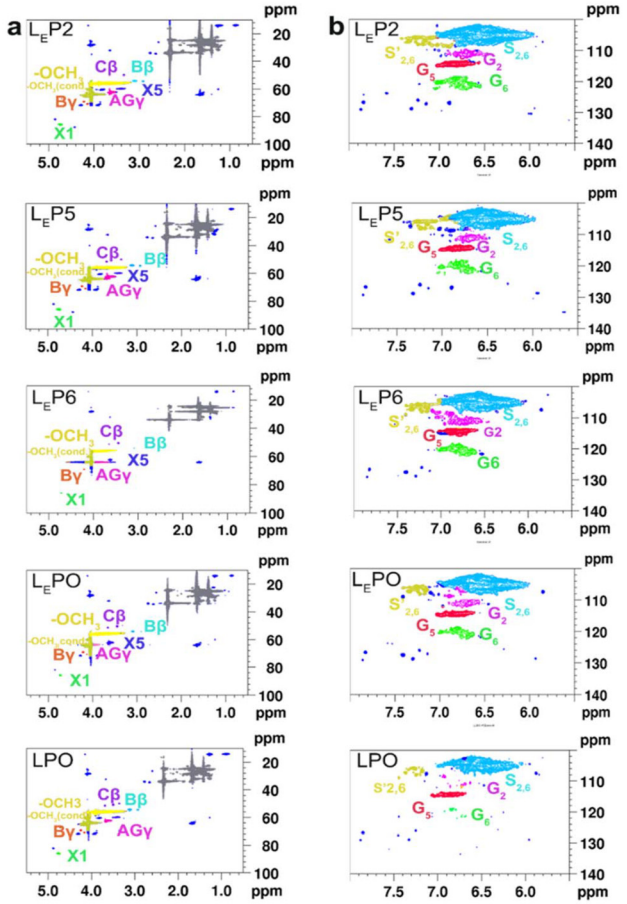

Fig. 3 HSQC NMR spectra, aliphatic region (a), and aromatic linkage regions (b) of L_EP2, L_EP5, L_EP6, L_EPO, and LPO.

regions had similar linkages to that of L_EPO. Aromatic linkage signals in L_EP2, L_EP5, L_EP6, and L_EPO results showed strong aromatic linkages, like L_E (Fig. 1g). This indicated that the lignin caprolactone polymers gained strong aliphatic signals due to CL grafting and polymerization while maintaining the lignin's aromatic structure. There is a decrease in the strength of the signal in LPO compared to L_EPO, notably for signals $S_{2,6}$, G_2, and G_6. The variation in the intensity of $S_{2,6}$, G_2, and G_6 may be attributed to the disparity in L and L_E (Fig. 1f and g). Furthermore, the $S_{2,6}$, G_2, and G_6 signals were weaker in LPO than in L. The decreased intensity can be related to potential shielding caused by PCL grafted on the neighboring aliphatic hydroxyl group of $S_{2,6}$, G_2, and G_6, as evidenced by ^{31}P NMR and the higher chain length of PCL in LPO as evidenced by higher DP (Table 1).

3.2.4. Molecular weight analysis. The M_w was investigated for L_EP2, L_EP5, L_EP6, L_EPO, and LPO samples (Table 1). The LPO polymer showed a higher molecular weight than L_EPO, which could have originated from the higher molecular weight of the pristine lignin (L). The molecular weight of the L_EP2, L_EP5, L_EP6, and L_EPO polymers increased significantly compared to L_E (Table 1), which further confirmed the introduction of an aliphatic polyester chain covalently bonded to the lignin structure (Fig. 2b). This indicated that there was a more significant reaction of lignin's hydroxyl (OH) groups and (ε-caprolactone) (CL) chains, which led to an increase in the M_w of the copolymers.

3.2.5. Thermal behavior. The thermal properties of L_EP2, L_EP5, L_EP6, L_EPO, and LPO polymers were analyzed using TGA and DSC (Fig. 4a). The TGA analysis for L_EP2, L_EP5, L_EP6, and L_EPO polymers showed a higher T_o, $T_{50\%}$, and DTG_{max} than L_E (Table 1). The thermal properties showed improvement by an elevated T_o for L_EPO and LPO compared to L_E and L.

This is due to the higher molecular weight of the polymers after lignin-caprolactone polymerization, which resulted in the grafting of PCL chains to the lignin backbone, improving its thermal stability (Table 1 or Fig. 4a and b). Similarly, the T_m of L_EP polymers was analyzed (Fig. 4c) and reported in Table 1. It is crucial to note that the T_m was recorded during the initial heating cycle of the DSC analysis due to the disappearance of the T_m in the last heating cycle. The disappearance of the T_m could result from the lower concentration of CL/OH (0.8–2.6 mmol), leading to a short PCL chain length (DP from Table 1) in the lignin molecular structure. Also, the shorter chain of PCL in lignin could experience restricted molecular mobility due to the random and rigid structure of lignin.[52] All the samples exhibited lower T_g (obtained from the second heating cycle of DSC) than L and L_E (Table S4†). The decreased T_g in the polymers may be attributed to increased free volume, allowing molecular movement due to the grafting of PCL on the lignin backbone.[52] Also, the difference in T_g and T_m between L_EP2, L_EP5, and L_EP6 is insignificant due to the greater lignin concentration in all the samples and the short chain length of PCL, as shown in Table 1.

3.2.6. Rheological assessment. The viscosity of lignin-caprolactone polymers at melt temperature as a function of shear rate was recorded in ramp-up experiments, as presented in Fig. 4d and Fig. S4.† The shear-thinning property is an essential characteristic of ink required for extrusion-based 3D printing. This feature was detected in L_EP6, L_EP5, L_EPO, and LPO (Fig. 4d). However, the L_EPO shows a lower viscosity at a lower shear rate, followed by LPO, L_EP5, and L_EP6. L_EPO's lower viscosity than LPO is attributed to the lower M_w and $Đ_M$ of L_E than L (Table 1). There is extensive evidence that greater M_w and a higher $Đ_M$ would result in more entanglements, a greater degree of intermolecular contacts, and the formation of a complex interplay of diverse flow behavior, leading to enhanced flow resistance.[53–55] During the ramp-up experiment at the melt temperature, L_EP2 exhibited a consistently low viscosity profile. The constant viscosity against a shear rate seen during the ramp-up experiment of L_EP2 may be attributed to the polymer's higher DP and M_w (Table 1). These factors contribute to a polymer without shear-thinning properties, which is not typical for a polymer suitable for 3D printing.[56] L_EP6 and L_EP5 exhibit shear-thinning behavior, making them attractive for 3D printing. Nevertheless, the notably elevated viscosity, even when subjected to a greater shear rate, may obstruct the nozzle, impeding the process of 3D printing by extrusion, making them undesirable for the FDM 3D printing

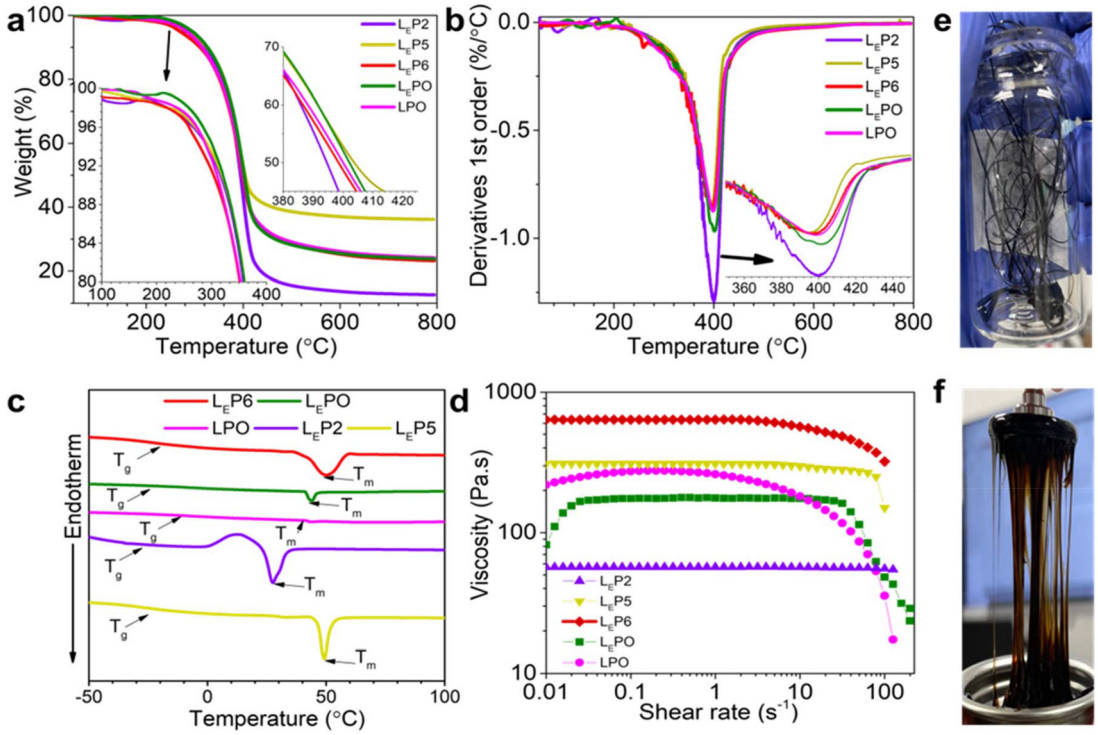

Fig. 4 TGA curve (a) and 1st order derivatives of TGA (b), glass transition (T_g) and melt temperature (T_m) (c) and viscosity at melt temperatures (d) and appearance of the sample LEPO at room temperature (e), and the melt temperature (f).

process.[57,58] Therefore, L_EP6 and L_EP5 were not used for further rheology analysis and 3D printing.

LPO and L_EPO were selected for further rheological analysis and 3D printing due to lower viscosity with a more shear-thinning behavior than the other samples, making them suitable candidates for FDM 3D printing. Temperature ramp and frequency sweep analysis provide information on molecular entanglement, molecular relaxation, layer stability, and guidelines of layer adhesion for FDM 3D printability.[59] The printability of L_EP and LPO was assessed using a temperature ramp experiment. The complex viscosity, storage (G'), and loss modulus (G'') decreased with reducing temperature for both polymers (Fig. 5a and b). The complex viscosity, G', and G'', of LPO were higher than those of L_EPO, which might be related to the higher M_w of LPO (Table 1). Furthermore, the point at which G' and G'' intersect (*i.e.*, cross-over point) appears at a lower temperature (55 °C) for LPO than for L_EPO (40 °C). This provides an insight into the material's behavior during printing, implying that LPO behaved more like a solid at a faster rate than L_EPO with the temperature decreasing. The loss modulus (G'') and storage modulus (G') of a polymer imply the layer adhesion and quality of 3D printable materials.[60] Strong interfacial bonding between layers is crucial for strong printing. An increment in the storage modulus often correlates with improved stiffness and better layer adhesion. Conversely, decreasing loss modulus may enhance printability by reducing energy dissipation during extrusion.[61] In this regard, L_EPO had a much more printable behavior than LPO. In addition, the ratio between G' and G'' (tan δ) of L_EPO was lower than that of LPO and closer to 1 (Fig. 5c). This indicates that L_EPO had more balanced viscous and elastic properties, *i.e.*, an ideal balance for FDM printing where a balanced flow during extrusion and shape retention after printing would be necessary.[62] In addition, the complex viscosity from the frequency sweep analysis in Fig. 5d exhibited that both polymers had similar flow behaviour, indicating that they could flow at their melting temperature in the printing nozzle in the extrusion step. However, the significantly higher viscosity of LPO could cause filament buckling during nozzle extrusion, which is typical for materials with a higher viscosity.[63] The final mechanical properties of the printed parts are directly dependent on the interlayer adhesion between the layers deposited subsequently. The adhesion between layers is determined by the diffusion of polymer chains across the interface and the reorganization of macromolecules to their initial state.[64] This process is directly influenced by the molten material's elastic or viscous properties and the polymer's relaxation time.[64,65] The frequency sweep analysis for both polymers shows $G'' > G'$ indicating an interlayer adhesion (Fig. 5e and f). In comparison, the LPO had a higher G' and G'' than L_EPO, indicating that LPO possessed more solid-like properties than L_EPO. The filaments were extruded using a filament extrusion machine, and the appearance of L_EPO and LPO is displayed in Fig. 5g and Fig. S7a.†

3.2.7. Mechanical and surface properties. The tensile strength of L_EPO was analyzed after the film was cast in a Mold

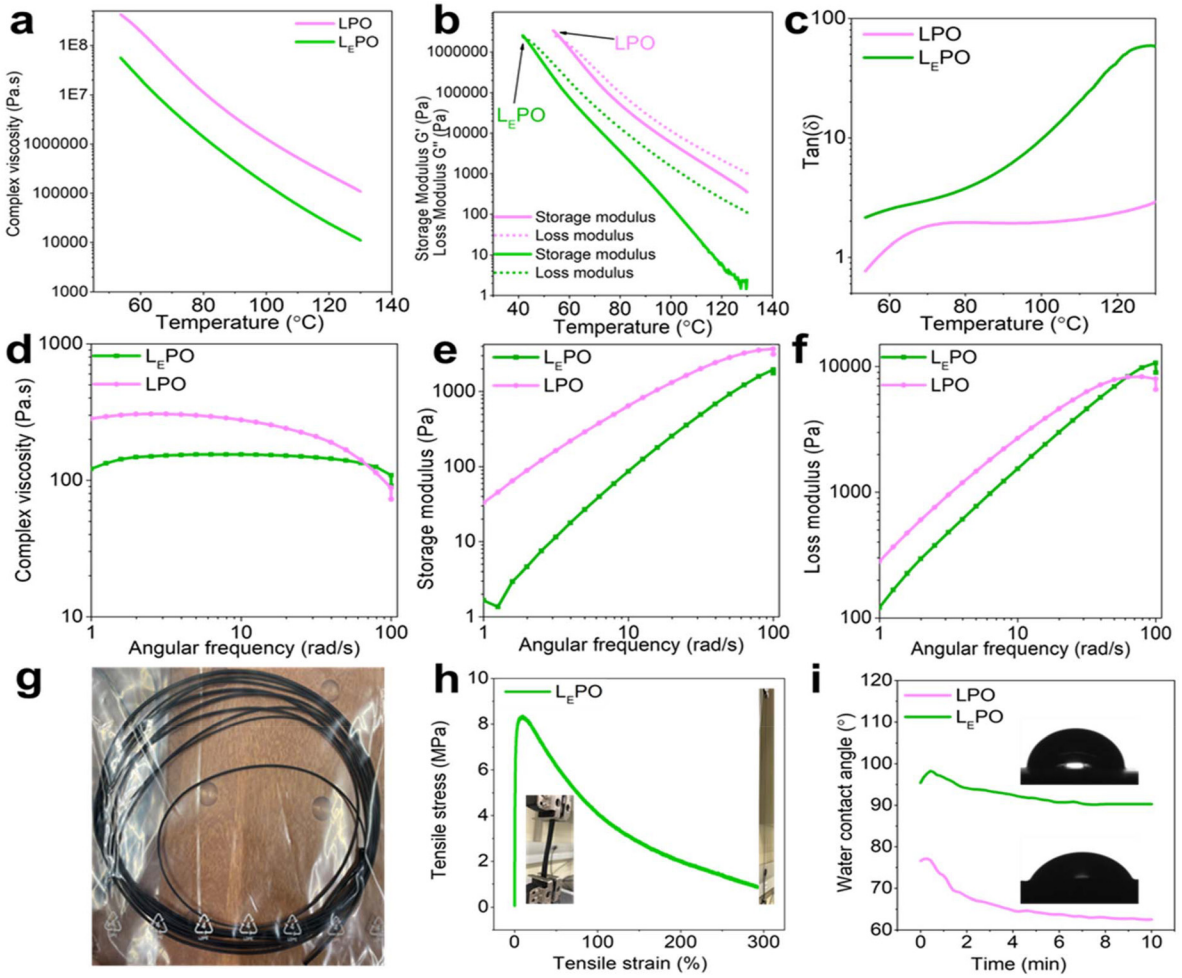

Fig. 5 Complex viscosity (a), storage and loss modulus (b), tan δ (c), of LPO and L_EPO from temperature ramp experiment, complex viscosity (d), storage modulus (e), loss modulus (f) from frequency sweep analysis: of LPO and L_EPO polymers and, extruded filament of (f), L_EPO polymer (g), tensile stress *vs.* strain curve (h), and water contact angle of L_EPO and LPO (i).

(Fig. 5h); however, the LPO film dried quickly, which hindered the film formation process (Fig. S7b†), and it became too brittle to be tested for tensile analysis. The poor mechanical properties of LPO can be attributed to several factors. Firstly, LPO has a higher molecular weight (Table 1), which leads to LPO having a higher viscosity at the melt temperature (Fig. 4d). Furthermore, LPO loses its elastic behavior and behaves more like a solid at a temperature higher than L_EPO, as evidenced by an earlier cross-over point in the temperature ramp experiment (Fig. 5b). That leads to faster drying and higher flow resistance at the melt temperature. The tensile strength of L_EPO was 0.9 ± 0.02 MPa, its elastic modulus was 277 ± 119%, and its young modulus was 2774 ± 1756 MPa. The water contact angle of L_EPO (92°) was higher than LPO (62°) (Fig. 5i), indicating the higher hydrophobicity of L_EPO, which could result from the higher percentage of substitution of the hydrophilic hydroxyl groups in L_EPO (67%) than LPO (51%) with PCL (Fig. S2†).

Overall, using several characterization methods clearly showed that ethanol fractionation had a noticeable effect on the physicochemical properties of the lignin-caprolactone polymer, as stated in the overall performance of LPO and L_EPO. The molecular weight, molecular weight distribution, and hydroxyl group content were altered due to ethanol separation, resulting in a lower molecular weight and increased hydroxyl groups. This led to L_E having a more significant advantage than L in interacting with CL, as seen by a higher grafting in the hydroxyl groups (Fig. S2†). L_EPO had a lower viscosity and better rheological, mechanical, and hydrophobic properties than LPO because it had a lower molecular weight (Table 1), which may be attributed to improved free volume for molecular chain mobility and conformational rearrangement. Table 2 shows that earlier publications have identified interfacial incompatibility between lignin and other polymers in the system. This incompatibility has restricted lignin's presence in the final products.

3.3. 3D printability of lignin-caprolactone polymer

The 3D printability of LPO and L_EPO was assessed using FDM, and images of the 3D printed parts are displayed in Fig. 6. The

Table 2 Literature results for the generation of lignin included caprolactone composites

Materials	Solvent	Filament preparation method	Lignin amount, wt%	Other components con. %	Viscosity, Pa S	Advantages	Shortcomings	Ref.
Lignin-caprolactone and acrylonitrile-butadiene-styrene	Solvent-free	Blending	5	ABS, 90 PCL, 5	2130	Lignin-PCL improved the processability of the composite	- Stability of composite material not reported - Lower concentration of lignin - Still used	66
Lignin, polycaprolactone, and curcumin	Solvent-free	Blending	10	Curcumin, 5 PCL, 85	NR	Lignin improved the antibacterial and antimicrobial properties	- Mechanical properties not reported - Lower concentration of lignin	67
Enzymatic lignin, polycaprolactone and polyurethane	Solvent-free	Blending	20	PCL, 30 PU, 55	100	Lignin enhanced the rigidity of the composite	Interface incompatibility between lignin and other components	68
Polylactic acid, polycaprolactone, and lignin	Solvent-free	Blending	2	PCL, 24 PLA, 65	NR	Lignin improved the thermal recovery and mechanical properties	Lower concentration of lignin	69
Lignin and caprolactone	Solvent-free	Copolymerization	75	Caprolactone, 25	160.9	- Higher concentration of lignin - Ease of use - Superior mechanical properties	Application of 3D printed material needs investigation	This work

pallets for both polymers were rolled, loaded, and printed using a 3D printer; however, as seen from the printed parts, a visible gap between layers indicates low interlayer diffusion and adhesion between deposited layers in the LPO samples (Fig. 6a′ and b′). Conversely, L_EPO showed no gaps between printed layers, indicating better interlayer adhesion and filling. This behavior could be attributed to the very high viscosity (Fig. 5a and d) and molecular weight of LPO (Table 1), inducing thermal crosslinking, which might lead to reducing molecular mobility and interfacial diffusion, thus reducing adhesion between deposited layers.[20]

Furthermore, the intersection point observed during the melt rheology investigation (Fig. 5b) of LPO occurred at higher temperatures (55 °C), indicating that the sample might lose its ability to melt more quickly when exposed to lower temperatures. This could hinder the bonding of layers, as seen in Fig. 6a′ and b′. The higher 3D printability of L_EPO than LPO might be ascribed to improved layer adhesion originating from the lowered molecular weight and viscosity of L_EPO due to L_E's lower molecular weight achieved by ethanol fractionation (Table 1). Therefore, we can conclude that the ethanol fractionation of alkali lignin improved the 3D printability of lignin-caprolactone polymers.

3.4. Implications

In the past, lignin polymers were used in 3D printing in polymer blends with other polymers, such as acrylonitrile-butadiene-styrene, polycaprolactone, cummin, polycaprolactone/polyurethane, and polylactic acid following the FDM-3D printing technique, as indicated in Table 2. The addition of lignin-caprolactone polymer (15 wt%) to acrylonitrile-butadiene-styrene led to a decrease in viscosity (2130 Pa s) compared to the formulations without lignin-caprolactone polymer (4270 Pa s) under similar temperatures and shear rates.[66] In another study, incorporating lignin-caprolactone polymer (40 wt%) into polycaprolactone and curcumin improved the blend's thermal stability even though the rheological properties were not reported.[67] Table 2 shows that earlier publications have identified interfacial incompatibility between lignin and other polymers in the system. This incompatibility has restricted lignin's presence in the final products. Utilizing a homogeneous copolymer would facilitate the manufacturing process. The current study is unique compared to the existing literature since the lignin-caprolactone polymer was used solitarily for 3D printing after mimicking the characteristics of lignin polymer *via* solvent fractionation (ethanol). The total concentration of lignin present in the lignin-caprolactone matrix was 75 wt% (*i.e.*, a truly sustainable material), based on the calculation in (eqn (S1)†), with much lower viscosity (160.9 Pa s) and ease of printing. Considering the ethanol fractionation, the overall use of lignin in the produced 3D printing material would be 40.12 wt% of the original pristine lignin. The results imply that almost 60% of pristine lignin is still available for other uses and can be incorporated into other value-added applications if collected after filtration. This study also conducted an analysis of variance (ANOVA) on the responses (viscosity, melt temperature, and degree of polymer-

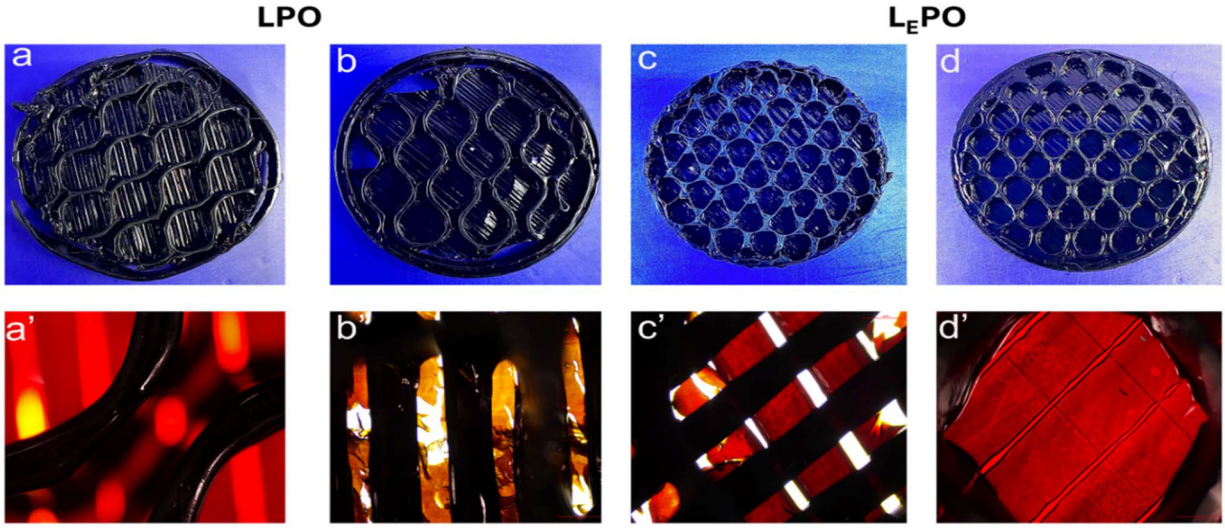

Fig. 6 FDM printed honeycomb structure of LPO photograph images of trial 1 (a) and trial 2 (b), light microscope image showing layer adhesions (a') and (b'), L_EPO photograph images of trial 1 (c), and trial 2 (d) and light microscope magnification showing layer adhesion (c') and (d').

ization) of lignin-caprolactone polymer, considering three variables: CL/OH ratio, reaction time, and catalyst concentration in Tables S5–S7.† The results indicate that all reaction parameters significantly affect the response variables, with *p*-values less than 0.05. Additionally, suitable models for predicting the response variables are presented, according to eqn (S10)–(S12).† This work provides an excellent insight into the use of lignin polymer for FDM-3D printing, which would reduce the use of inorganic and synthetic polymers in 3D printed materials, tackling the problem of sustainability. Future research may explore the substitutions of hexane with a more environmentally friendly solvent utilized for the extraction of extractives from post-ethanol fractionated lignin, as well as the DBTDL catalyst with environmentally friendly catalysts.

4. Conclusion

This work aimed to reduce the molecular weight and molecular weight distribution of birch alkali lignin (L) *via* ethanol fraction before polymerization of the fractionated lignin (L_E) with caprolactone for FDM-3D printing. L_E showed a higher hydroxyl group content, lower molecular weight, and lower poly dispersibility than L. The increase in hydroxyl groups created more reactive sites on the lignin structure for the caprolactone grafting. The copolymerization of L_E and caprolactone was optimized by considering the melt temperature (T_m), degree of polymerization (DP), and viscosity as the primary factors of its printability. The results confirmed that the optimized sample (L_EPO), produced by a CL/OH ratio of 1.15 mmol g^{-1}, a reaction duration of 420 minutes, and a catalyst concentration of 1 wt% showed better printability with a melt temperature of 48 °C, shear-thinning behavior, low viscosity (160.9 Pa s) and better thermal stability with an onset temperature 292.2 °C. The melt rheology results demonstrated that L_EPO exhibited superior interlayer adhesion during printing and mechanical capabilities to unfractionated lignin-caprolactone (LPO) polymer. L_E's decreased molecular weight and narrower molecular weight distribution contributed to L_EPO's reduced viscosity. Furthermore, the occurrence of the cross-over points between G' and G'' appearing 15 °C higher than LPO provided L_EPO with a favorable condition for improved layer formation and enhanced bonding between layers. L_EPO's water contact angle value was higher than those of LPO by 30°, which was consistent with the higher grafting percentage of CL (11% higher) to the hydroxyl groups of L_EPO than LPO. Based on this study's findings, the reduced variability in the lignin structure after ethanol fractionation of lignin is a viable approach for producing lignin-caprolactone polymer for 3D printable materials, where 75% of the fractionated lignin (representing 40.12% unfractionated pristine alkali birch lignin) was part of the lignin-caprolactone polymer. More extensive research is required to explore the usefulness of this 3D-printed lignin-caprolactone polymer in areas such as bio-medical applications.

Author contributions

Banchamlak Bemerw Kassaun: writing the original draft, conceptualization, methodology, and investigation. Luyao Wang: methodology, investigation. Oskar Backman: methodology, investigation. Chunlin Xu: writing-review & editing, project administration, methodology, investigation, conceptualization; Pedram Fatehi: writing-review and editing, project administration, methodology, investigation, conceptualization.

Data availability

The data supporting this article have been included as part of the ESI.† No software or codes were used in this article, and

extra data can be obtained upon request from the corresponding author.

Conflicts of interest

The authors declare that they have no competing interests.

Acknowledgements

The authors acknowledge the Globalink MITACS national research organization, Northern Ontario Heritage Fund Corporation, NSERC, Business Finland (project 43674/31/2020), and part of the research used Research Council of Finland Research Infrastructure "Printed Intelligence Infrastructure kkjure" (PII-FIRI).

References

1 T. Yao, J. Ye, Z. Deng, K. Zhang, Y. Ma and H. Ouyang, *Composites, Part B*, 2020, **188**, 107894.
2 S. Garzon-Hernandez, A. Arias and D. Garcia-Gonzalez, *Composites, Part B*, 2020, **201**, 108373.
3 Z. Fu, S. Naghieh, C. Xu, C. Wang, W. Sun and X. Chen, *Biofabrication*, 2021, **13**, 033001.
4 N. R. Madhu, H. Erfani, S. Jadoun, M. Amir, Y. Thiagarajan and N. P. S. Chauhan, *Int. J. Adv. Manuf. Technol.*, 2022, **122**, 2125–2138.
5 L. Shao, Y.-C. Chang, C. Hao, M.-E. Fei, B. Zhao, B. J. Bliss and J. Zhang, *Green Chem.*, 2022, **24**, 8716–8724.
6 Y. Bozkurt and E. Karayel, *J. Mater. Res. Technol.*, 2021, **14**, 1430–1450.
7 G. Chyr and J. M. DeSimone, *Green Chem.*, 2023, **25**, 453–466.
8 S. Shariatnia, A. Veldanda, S. Obeidat, D. Jarrahbashi and A. Asadi, *Composites, Part B*, 2019, **177**, 107291.
9 Ö. Yapar, in *Additive Manufacturing in Multidisciplinary Cooperation and Production*, Springer, 2023, pp. 79–102. DOI: 10.1007/978-3-031-37671-9_8.
10 D. S. Bajwa, G. Pourhashem, A. H. Ullah and S. G. Bajwa, *Ind. Crops Prod.*, 2019, **139**, 111526.
11 S. Wasti, E. Triggs, R. Farag, M. Auad, S. Adhikari, D. Bajwa, M. Li and A. J. Ragauskas, *Composites, Part B*, 2021, **205**, 108483.
12 A. E. Kazzaz, Z. H. Feizi and P. Fatehi, *Green Chem.*, 2019, **21**, 5714–5752.
13 O. Yu and K. H. Kim, *Appl. Sci.*, 2020, **10**, 4626.
14 M. Fazeli, S. Mukherjee, H. Baniasadi, R. Abidnejad, M. Mujtaba, J. Lipponen, J. Seppälä and O. J. Rojas, *Green Chem.*, 2024, **26**, 593–630.
15 V. Mimini, E. Sykacek, S. N. A. Syed Hashim, J. Holzweber, H. Hettegger, K. Fackler, A. Potthast, N. Mundigler and T. Rosenau, *J. Wood Chem. Technol.*, 2019, **39**, 14–30.
16 X. Zhang, M. Morits, C. Jonkergouw, A. Ora, J. J. Valle-Delgado, M. Farooq, R. Ajdary, S. Huan, M. Linder and O. Rojas, *Biomacromolecules*, 2020, **21**, 1875–1885.
17 N. A. Nguyen, S. H. Barnes, C. C. Bowland, K. M. Meek, K. C. Littrell, J. K. Keum and A. K. Naskar, *Sci. Adv.*, 2018, **4**, eaat4967.
18 J. Domínguez-Robles, N. K. Martin, M. L. Fong, S. A. Stewart, N. J. Irwin, M. I. Rial-Hermida, R. F. Donnelly and E. Larrañeta, *Pharmaceutics*, 2019, **11**, 165.
19 S. Wasti, E. Triggs, R. Farag, M. Auad, S. Adhikari, D. Bajwa, M. Li and A. J. Ragauskas, *Composites, Part B*, 2021, **205**, 108483.
20 N. A. Nguyen, C. C. Bowland and A. K. Naskar, *Appl. Mater. Today*, 2018, **12**, 138–152.
21 P. Schlee, O. Hosseinaei, C. A. O'Keefe, M. J. Mostazo-López, D. Cazorla-Amorós, S. Herou, P. Tomani, C. P. Grey and M.-M. Titirici, *J. Mater. Chem.*, 2020, **8**, 23543–23554.
22 L. S. Ebers, A. Arya, C. C. Bowland, W. G. Glasser, S. C. Chmely, A. K. Naskar and M. P. Laborie, *Biopolymers*, 2021, **112**, e23431.
23 V. V. Adithyamol, S. Gupta and B. Kandasdubramanian, *Biomed. Mater. Devices*, 2024, 1–13, DOI: 10.1007/s44174-024-00193-1.
24 H. Ye, Y. He, H. Li, T. You and F. Xu, *Polymers*, 2023, **15**, 2806.
25 M. Labet and W. Thielemans, *Chem. Soc. Rev.*, 2009, **38**, 3484–3504.
26 R. M. Mohamed and K. Yusoh, *Adv. Mater. Res.*, 2016, **1134**, 249–255.
27 M. Bartnikowski, T. R. Dargaville, S. Ivanovski and D. W. Hutmacher, *Prog. Polym. Sci.*, 2019, **96**, 1–20.
28 V. Guarino, G. Gentile, L. Sorrentino and L. Ambrosio, *EPST*, 2002, pp. 1–36. DOI: 10.1002/0471440264.pst658.
29 C. M. B. Ho, A. Mishra, P. T. P. Lin, S. H. Ng, W. Y. Yeong, Y. J. Kim and Y. J. Yoon, *Macromol. Biosci.*, 2017, **17**, 1600250.
30 W. Wang, G. F. Caetano, W.-H. Chiang, A. L. Braz, J. J. Blaker, M. A. C. Frade and P. J. Bártolo, *Int. J. Bioprint.*, 2016, **2**, 95–104.
31 K. Liu, J. Sun, Q. Zhu, X. Jin, Z. Zhang, Z. Zhao, G. Chen, C. Wang, H. Jiang and P. Zhang, *Ceram. Int.*, 2022, **48**, 24032–24043.
32 Z. Muwaffak, A. Goyanes, V. Clark, A. W. Basit, S. T. Hilton and S. Gaisford, *Int. J. Pharm.*, 2017, **527**, 161–170.
33 I.-K. Park, H. Sun, S.-H. Kim, Y. Kim, G. E. Kim, Y. Lee, T. Kim, H. R. Choi, J. Suhr and J.-D. Nam, *Sci. Rep.*, 2019, **9**, 7033.
34 K. L. Kadam, C. Y. Chin and L. W. Brown, *Environ. Prog. Sustainable Energy*, 2009, **28**, 89–99.
35 H. Sadeghifar and A. Ragauskas, *ACS Sustainable Chem. Eng.*, 2020, **8**, 8086–8101.
36 Y. Wang, L. Wei, Q. Hou, Z. Mo, X. Liu and W. Li, *Fermentation*, 2023, **9**, 386.
37 C. A. E. Costa, F. M. Casimiro, C. Vega-Aguilar and A. E. Rodrigues, *ChemEngineering*, 2023, **7**, 42.
38 R. Liu, A. Smeds, L. Wang, A. Pranovich, J. Hemming, S. Willfor, H. Zhang and C. Xu, *ACS Sustainable Chem. Eng.*, 2021, **9**, 13862–13873.

39 L. Wang, L. Lagerquist, Y. Zhang, R. Koppolu, T. Tirri, I. Sulaeva, S. V. Schoultz, L. Vähäsalo, A. Pranovich and T. Rosenau, *ACS Sustainable Chem. Eng.*, 2020, **8**, 13517–13526.
40 C. Gao, M. Li, C. Zhu, Y. Hu, T. Shen, M. Li, X. Ji, G. Lyu and W. Zhuang, *Composites, Part B*, 2021, **205**, 108530.
41 G. Zinovyev, I. Sulaeva, S. Podzimek, D. Rössner, I. Kilpeläinen, I. Sumerskii, T. Rosenau and A. Potthast, *ChemSusChem*, 2018, **11**, 3259–3268.
42 X. Meng, C. Crestini, H. Ben, N. Hao, Y. Pu, A. J. Ragauskas and D. S. Argyropoulos, *Nat. Protoc.*, 2019, **14**, 2627–2647.
43 D. Diment, O. Tkachenko, P. Schlee, N. Kohlhuber, A. Potthast, T. M. Budnyak, D. Rigo and M. Balakshin, *Biomacromolecules*, 2023, **25**, 200–212.
44 M. Gigli and C. Crestini, *Green Chem.*, 2020, **22**, 4722–4746.
45 R. Liu, A. Smeds, T. Tirri, H. Zhang, S. Willfor and C. Xu, *ACS Sustainable Chem. Eng.*, 2022, **10**, 14588–14599.
46 M. Sette, R. Wechselberger and C. Crestini, *Chem. – Eur. J.*, 2011, **17**, 9529–9535.
47 T. Pang, G. Wang, H. Sun, W. Sui and C. Si, *Ind. Crops Prod.*, 2021, **165**, 113442.
48 J.-H. Choi, S.-M. Cho, J.-C. Kim, S.-W. Park, Y.-M. Cho, B. Koo, H. W. Kwak and I.-G. Choi, *ACS Omega*, 2021, **6**, 1534–1546.
49 N. A. Nguyen, K. M. Meek, C. C. Bowland and A. K. Naskar, *Data Brief*, 2019, **22**, 392–399.
50 M. C. Najarro, M. Nikolic, J. Iruthayaraj and I. Johannsen, *ACS Appl. Polym. Mater.*, 2020, **2**, 5767–5778.
51 E. A. Capanema, M. Y. Balakshin and J. F. Kadla, *J. Agric. Food Chem.*, 2004, **52**, 1850–1860.
52 T. Hatakeyama, S. Yamashita and H. Hatakeyama, *J. Therm. Anal. Calorim.*, 2021, **143**, 203–211.
53 J. F. Vega, J. Otegui, J. Ramos and J. Martínez-Salazar, *Rheol. Acta*, 2012, **51**, 81–87.
54 S. Middleman, *J. Appl. Polym. Sci.*, 1967, **11**, 417–424.
55 S. J. Kozmiski, *Effect of Molecular Weight Distribution on Viscosity-shear Rate and Die Swell Behavior in Homologous Polystyrene Blends*, The Pennsylvania State University, 1984.
56 S. Wickramasinghe, T. Do and P. Tran, *Polymers*, 2020, **12**, 1529.
57 Y. Tlegenov, W. F. Lu and G. S. Hong, *Prog. Addit. Manuf.*, 2019, **4**, 211–223.
58 H. Zhang, L. Zhang, H. Zhang, J. Wu, X. An and D. Yang, *Int. J. Adv. Manuf. Technol.*, 2021, **117**, 3549–3562.
59 M. V. Candal, I. Calafel, N. Aranburu, M. Fernández, G. Gerrica-Echevarria, A. Santamaría and A. J. Müller, *Addit. Manuf.*, 2020, **36**, 101408.
60 A. Patti, S. Acierno, G. Cicala and D. Acierno, *ChemEngineering*, 2022, **7**, 1.
61 S. Thumsorn, W. Prasong, T. Kurose, A. Ishigami, Y. Kobayashi and H. Ito, *Polymers*, 2022, **14**, 2721.
62 R. Arrigo and A. Frache, *Polymers*, 2022, **14**, 1754.
63 K. Ilyés, N. K. Kovács, A. Balogh, E. Borbás, B. Farkas, T. Casian, G. Marosi, I. Tomuță and Z. K. Nagy, *Eur. J. Pharm. Sci.*, 2019, **129**, 110–123.
64 A. Das, J. A. Riet, M. J. Bortner and C. McIlroy, *Phys. Fluids*, 2022, **34**, 123108.
65 Y. Weng, M. Li, D. Zhang, M. J. Tan and S. Qian, *Cem. Concr. Res.*, 2021, **143**, 106386.
66 S.-H. Kim, K. Choi, H. R. Choi, T. Kim, J. Suhr, K. J. Kim, H. J. Choi and J.-D. Nam, *ACS Omega*, 2019, **4**, 10036–10043.
67 J. Domínguez-Robles, E. Cuartas-Gómez, S. Dynes, E. Utomo, Q. K. Anjani, U. Detamornrat, R. F. Donnelly, N. Moreno-Castellanos and E. Larrañeta, *Sustainable Mater. Technol.*, 2023, **35**, e00581.
68 F. Suo, X. Bai, Y. Liu, M. Xu, T. Gu, L. Cao, X. Lv, X. Zhang and Y. Yao, *Int. J. Biol. Macromol.*, 2024, 132943, DOI: **10.1016/j.ijbiomac.2024.132943**.
69 B. Liu, X. Gu, X. Chen, Y. Yang, J. Zou, H. Yin and Y. Cai, *J. Appl. Polym. Sci.*, 2024, **141**, e55252.